Protein Engineering, Design & Selection, 2018, vol. 31 no. 7-8, pp. 289–299
doi: 10.1093/protein/gzy021
Advance Access Publication Date: 28 August 2018
Original Article

OXFORD

Original Article

Variable heavy–variable light domain and Fab-arm CrossMabs with charged residue exchanges to enforce correct light chain assembly

Joerg Thomas Regula[1], Sabine Imhof-Jung[1], Michael Mølhøj[1], Joerg Benz[2], Andreas Ehler[2], Alexander Bujotzek[1], Wolfgang Schaefer[1], and Christian Klein[3,*]

[1]Roche Pharmaceutical Research and Early Development, Large Molecule Research, Roche Innovation Center Munich, Penzberg, Germany, [2]Roche Pharmaceutical Research and Early Development, Chemical Biology, Roche Innovation Center Basel, Basel, Switzerland, and [3]Roche Pharmaceutical Research and Early Development, Discovery Oncology, Roche Innovation Center Zurich, Schlieren, Switzerland

[*]To whom correspondence should be addressed. E-mail: christian.klein.ck1@roche.com
Edited by Andrew Bradbury, Board Member for PEDS

Received 19 April 2018; Revised 26 July 2018; Editorial Decision 1 August 2018; Accepted 3 August 2018

Abstract

Technologies for the production of bispecific antibodies need to overcome two major challenges. The first one is correct heavy chain assembly, which was solved by knobs-into-holes technology or charge interactions in the CH3 domains. The second challenge is correct light chain assembly. This can be solved by engineering the Fab-arm interfaces or applying the immunoglobulin domain crossover approach. There are three different crossovers possible, namely Fab-arm, constant domain and variable domain crossovers. The CrossMab$^{CH1–CL}$ exchange does not lead to the formation of unexpected side products, whereas the CrossMab^{Fab} and the CrossMab$^{VH–VL}$ formats result in the formation of typical side products. Thus, CrossMab$^{CH1–CL}$ was initially favored for therapeutic antibody development. Here, we report a novel improved CrossMab design principle making use of site-specific positional exchanges of charged amino acid pairs in the constant domain of these CrossMabs to enable the correct light chain assembly in the CrossMab$^{VH–VL}$ and improvements for the CrossMab^{Fab} design.

Key words: Angiopoietin-2, bispecific antibody, CrossMab, VEGF

Introduction

The idea of bispecific antibodies and their potential to efficiently treat diseases attracted researchers almost since the invention of monoclonal antibodies. The first approvals of the bispecific antibodies like catumaxomab (Chelius *et al.*, 2010), blinatumomab (Nagorsen *et al.*, 2012), emicizumab (Kitazawa *et al.*, 2017; Oldenburg *et al.*, 2017) and various bispecific molecules in advanced clinical development (Brinkmann and Kontermann, 2017; Verdino *et al.*, 2018), underline the maturity of this field of research. The underlying technologies to design and manufacture bispecific antibodies are manifold and have enabled industrial scale production (Spiess *et al.*, 2015; Brinkmann and Kontermann, 2017; Krah *et al.*, 2017; Verdino *et al.*, 2018). This is reflected in the increasing number of first in man trials with this class of molecules (Brinkmann and Kontermann, 2017; Mullard, 2017).

In 2011, we reported the principle of domain crossover IgG-format antibodies as a generic principle to produce bispecific

© The Author(s) 2018. Published by Oxford University Press.

This is an Open Access article distributed under the terms of the Creative Commons Attribution Non-Commercial License (http://creativecommons.org/licenses/by-nc/4.0/), which permits non-commercial re-use, distribution, and reproduction in any medium, provided the original work is properly cited. For commercial re-use, please contact journals.permissions@oup.com

antibodies (Schaefer *et al.*, 2011; Klein *et al.*, 2012). The principle is based on the domain exchange/positional exchange of one complete Fab (Fragment antigen binding) arm, or individual domains within one of the Fab binding arms. These simple positional exchanges aimed to exclude the possibility of light chain mispairing by an alteration of the symmetry of the bispecific antibody. There are three general possibilities for the domain crossover: The most obvious exchange is the translocation of the light chain in the former position of the heavy chain Fab on one side of the antibody, termed CrossMab^{Fab}. Alternatively, the variable domains (variable heavy: VH, variable light: VL) or the constant domains (constant heavy 1: CH1, constant light: CL) can be exchanged resulting in the CrossMab$^{VH–VL}$ or CrossMab$^{CH1–CL}$, respectively. For these two CrossMab versions the elbow region differs from the natural amino acid sequence (Schaefer *et al.*, 2011; Klein *et al.*, 2012). Consequently, it is required to design the new elbow region as its length differs on the light and heavy side of the originating Fab. There are many elbow sequences possible and optimized elbow sequences were recently published (see also Table I) (Klein *et al.*, 2016). Typically, the crossover principle is independent of the elbow sequences, while alterations in these sequences may sometimes impact stability and the light chain pairing selectivity. Our experimental data from all three CrossMab designs indicate that the recommended sequences show a beneficial side product profile and less non-cognate light chain pairings than a bispecific antibody simply using knobs-into-holes and two unmodified light chains (Schaefer *et al.*, 2011, 2016). Nevertheless, based on the theoretical domain interactions only for the CrossMab$^{CH1–CL}$, no relevant amount of non-cognate light chain pairings can be expected. Consequently, this CrossMab design has already been used for currently four clinical stage bispecific CrossMabs of 1 + 1, 2 + 1 and 2 + 2 valencies (Kienast *et al.*, 2013; Brunker *et al.*, 2016; Lehmann *et al.*, 2016; Regula *et al.*, 2016, 2017; Bacac *et al.*, 2016a, 2016b) and also been applied by academic groups for the development of bispecific molecules (Klein *et al.*, 2016). Since the first conceptual CrossMab design experiments we tried to understand the driving forces for correct light chain assembly and the root cause of side product formation to enable efficient use of the Fab-arm exchange and the variable domain exchange as an alternative to the CH1–CL crossover. The main side-product of the CrossMab^{Fab} is a non-functional one-armed monovalent antibody (MoAb), which forms by heterodimerization of the two different heavy chains. For the CrossMab$^{VH–VL}$, a Bence-Jones like product can be assembled by adding the same non-crossed light chain twice to the formed heavy chain heterodimer (Klein *et al.*, 2016), resulting in both cases above in a non-cognate light chain assembly. The understanding of the root-cause of their assembly enables the improvements based on rational design.

Table I. Typical and recommended elbow sequences for kappa and lambda domain cross-overs

Wildtype elbow sequences	
VH-CH1	LVTVSSASTKGPSV
Vκ-Cκ	KVEIK-RTVAAPSV
Vλ-Cλ	KVTVLGQPKAAPSV
Kappa crossover	
Vκ-CH1	KVEIK-SSAS-TKGPSV
VH-Ck	LVVTV-SSAS-VAAPSV
Vκ-CH1	KVESK-SSAS-TKGPSV
VH-Ck	LVVTV-SSRT-VAAPSV
Lambda crossover	
Vλ-CH1	KVTVL-SSAS-TKGPSV
VH-Cλ	LVVTV-SGQP-KAAPSV

The introduction or the modification of electrostatic or hydrophobic interactions, as well as steric hindrance is key elements in the modern protein engineering toolbox. These modifications can be applied to the variable and constant domains. The most well-known approach is the knobs-into-holes modification which ensures correct heavy chain heterodimers in bispecific antibodies (Merchant *et al.*, 1998). Igawa *et al.* reported the improved expression of a single chain diabody directed against the thrombopoietin receptor by the mutation of glutamine at V_H(39) and V_L(38) into V_H(39E) and V_L(38 K) in one scFv and vice versa in the second one to ensure the diabody assembly and not the tandem scFv conformation (Igawa *et al.*, 2010). Liu *et al.* reported the modification of the VH-CH1 and VL-CK interface with opposite charges in each Fab arm (Liu *et al.*, 2015). The combination of computational and rational design helped Lewis *et al.* to develop orthogonal Fab interfaces to express correctly assembling bispecific antibodies with four individual chains (Lewis *et al.*, 2014). As a matter of fact, today, there are many different solutions to generate heterodimeric bispecific antibodies utilizing the IgG scaffold. Here, we report improvements on the CrossMab technology for the CrossMab^{Fab} and $^{VH–VL}$ to prevent non-cognate light chain pairings via inversion of existing charged residue pairs in the constant Fab domains.

Material and Methods

Ang-2-VEGF CrossMabs

The Ang-2-VEGF CrossMabs for this publication were previously described (Schaefer *et al.*, 2011; Fenn *et al.*, 2013). Briefly, CrossMabs were generated by the appropriate domain cross-over in the VEGF binding Fab arm combined with knob-into-holes modification with hole on the VEGF binding heavy chain, whereas the Ang-2 side remained unmodified in the Fab region and contained the knob modification (Kuglstatter *et al.*, 2017). The sequences including highlighted sites of modification were attached in the supplement.

Recombinant expression of CrossMab antibodies

All antibody HC and LC genes were ordered as synthetic gene fragments and cloned via unique restriction sites using standard cloning procedures into separate expression vectors for each chain enabling secretory expression in HEK cells growing in suspension. The KiH mutations described by Carter and colleagues were used (Knob: T366W; Hole: T366S, L368A, and Y407V) (Merchant *et al.*, 1998). In addition, two Cys residues were introduced in the CH3 domains (S354C in the knob chain and Y349C in the hole chain) that form a stabilizing disulfide bridge (Carter, 2001; Kuglstatter *et al.*, 2017). Transfection (1:1:1:1 plasmid ratios) into HEK293-F cells (Invitrogen, 510029) was performed according to the cell supplier's instructions using Maxiprep (Qiagen, 12163) preparations of the antibody vectors, Opti-MEM I medium (Invitrogen, 31985) 293fectin (Invitrogen, 31985070), and an initial cell density of 1–2 × 10^6 viable cells/ml in serum free FreeStyle 293 expression medium (Invitrogen, 12338018). Antibody containing cell culture supernatants were harvested after 7 days of cultivation in shake flasks by centrifugation at 14 000 × *g* for 30 min and filtered through a 0.22 µm sterile filter (Thermo Scientific, 566–0020). The antibodies were purified directly from the supernatant, or the supernatant was stored at −80°C until purification.

Protein purification

Proteins were purified from filtered cell culture supernatants referring to standard protein A protocols. The antibodies were captured

by affinity chromatography using HiTrap MabSelect SuRe (GE Healthcare, 11–0034–93) equilibrated with PBS. Elution of antibodies was achieved at pH 3.0 followed by immediate neutralization of the sample. Aggregated protein, or in the case of the CrossMab^{Fab} a light chain heterodimer, was separated from monomeric antibodies by size exclusion chromatography (Superdex 200; GE Healthcare, 17–5175–01) in 20 mM histidine, 140 mM NaCl, pH 6.0. Monomeric antibody fractions were pooled, concentrated if required using a 30 kDa molecular weight cut-off Millipore Amicon Ultra (Millipore, UFC803096) centrifugal concentrator, and stored at −80°C.

Protein concentration determination

The protein concentration was determined by the optical density (OD) at 280 nm, using the molar extinction coefficient calculated on the basis of the amino acid sequence.

Capillary electrophoresis

Purity and antibody integrity were analyzed by CE-SDS using microfluidic Labchip technology (PerkinElmer, USA). Five microliter of protein solution was prepared for CE-SDS analysis using the HT Protein Express Reagent Kit according to the manufacturer's instructions and analyzed on a LabChip GXII system using a HT Protein Express Chip. Data were analyzed using the LabChip GX Software.

Aggregation onset temperature/dynamic light scattering

Samples were prepared at 1 mg/ml in 20 mM Histidine chloride, 140 mM NaCl, pH 6.0. In a 384-well plate, 40 µl sample was filtered through a 0.4 µm filter, overlaid with 20 µl of paraffin oil and heated in a DynaPro plate reader (Wyatt Inc., Santa Barbara, USA) from 25°C to 80°C at a rate of 0.02°C/min. DLS data were recorded continuously and plotted against the temperature. The aggregation onset temperature (T_{agg}) is defined as the temperature at which the average hydrodynamic radius begins to increase.

Analytical size exclusion chromatography

Size exclusion chromatography (SEC) for the determination of the aggregation and oligomeric state of antibodies was performed by HPLC chromatography. Briefly, Protein A purified antibodies were applied to a Tosoh TSKgel G3000SW column in 300 mM NaCl, 50 mM KH_2PO_4/K_2HPO_4, pH 7.5 on an Dionex Ultimate® system (Thermo Fischer Scientific) or to a Superdex 200 column (GE Healthcare) in 2 × PBS on a Dionex HPLC-System. The eluted protein was quantified by UV absorbance and integration of peak areas. BioRad Gel Filtration Standard 151–1901 served as a standard.

Thermal stability (aggregation onset temperature)

Samples were prepared at 1 mg/ml in 20 mM histidine chloride, 140 mM NaCl, pH 6.0 and transferred in a 9 µl multi-cuvette array. The multi-cuvette array was heated from 35°C to 90°C at a constant rate of 0.1°C/min in an Optim1000 instrument (Avacta Analytical Inc.). The instrument continuously records the intensity of scattered light of a 266 nm laser with a data point approximately every 0.5°C. Light scattering intensities were plotted against the temperature. The aggregation onset temperature (T_{agg}) is defined as the temperature at which the scattered light intensity begins to increase.

The melting temperature T_m, was assessed by recording the intrinsic Tryptophan fluorescence with an Optim1000 instrument (Avacta Analytical Inc.). Samples were prepared at ~1 mg/ml in 20 mM His, 140 mM NaCl pH 6.0 and transferred to a 9 µl multi-cuvette array. The multi-cuvette array was heated from 30°C to 90°C at a constant rate of 0.1°C/min. The instrument continuously records fluorescence emission spectra after excitation with a 266 nm laser, providing a data point approximately every 0.6°C. The melting temperature, T_m, is determined by plotting the fluorescence intensity against the temperature and T_m is defined as the inflection point in these curves.

UHR-ESI-QTOF mass spectrometry

The correct assembly of the CrossMab antibodies was analyzed by electrospray ionization mass spectrometry of deglycosylated and deglycosylated/limited LysC digested molecules. 100 µg antibody was deglycosylated with *N*-Glycosidase F (Roche, 11 836 552 001) at 37°C for 16 h in a 100 mM phosphate buffer and subsequently denatured with 2 M Guanidinium-HCl at 37°C for 30 min. The limited LysC (Roche) digestions were performed with 100 µg deglycosylated CrossMabs in a Tris buffer pH 8 at 37°C for 40 min. Subsequently, the samples were desalted by HPLC on a Sephadex G25 column (GE Healthcare, 17–0032–02) using 40% acetonitrile with 2% formic acid (v/v). The total mass was determined by UHR-ESI-QTOF mass spectrometry on a maXis 4 G UHR-QTOF MS system (Bruker Daltonik) equipped with a TriVersa NanoMate source (Advion). Calibration was performed with sodium iodide (Tof G2-Sample Kit 2; Waters). Data acquisition was done at 1000–4000*m/z* (ISCID: 130.0 eV) and 600–2000*m/z* (ISCID: 0.0 eV) for the deglycosylated and deglycosylated/limited LysC digested CrossMabs, respectively. The raw mass spectra were evaluated and transformed into individual relative molar masses using an in-house developed software tool. The quantitative evaluation of the mass spectra was performed by summing up contributions of *m/z* ion intensities of all charge states forming the dominant part (larger than 20%) of the charge state envelope as observed for the most abundant individual product mass. Then all peak contributions (fitted as Gaussians) of all signals in these charge states were used to calculate the relative contents of the individual species.

Functional characterization

Determination of binding and binding affinity of multispecific antibodies to the respective antigens using surface plasmon resonance (SPR) (BIACORE®, GE Healthcare).

Assessment of VEGF binding

Binding of indicated antibodies to human VEGFA-121 was investigated by surface plasmon resonance using a BIACORE® T200 instrument (GE Healthcare). Around 10 000 (RU) of anti His antibody (1 µg/ml anti His antibody; Order Code: 28995056; GE Healthcare Bio-Sciences AB, Sweden) were coupled on a Series S CM5 chip (GE Healthcare BR-1005-30) at pH 5.0 by using an amine coupling kit supplied by the GE Healthcare. HBS-N (10 mM HEPES, 150 mM NaCl pH 7.4, GE Healthcare) was used as running buffer during the immobilization procedure. For the following kinetic characterization, sample and running buffer was PBS-T (10 mM phosphate buffered saline including 0.05% Tween20) at pH 7.4. The flow cell was set to 25°C – and the sample block set to 12°C – and primed with running buffer twice prior to kinetic characterization.

VEGF-A-121-His was captured by injecting a 0.5 µg/ml solution for 30 s at a flow of 5 µl/min. The association was measured by injection of the indicated antibodies in various concentrations in solution for 180 s at a flow of 30 µl/min starting with 1000 nM in 1:3 serial dilutions. The dissociation phase was monitored for up to 600 s and triggered by switching from the sample solution to running buffer. The surface was regenerated by 60 s washing with a Glycine pH 1.5 solution at a flow rate of 30 µl/min. Sensorgrams were double referenced by subtracting both anti His antibody and buffer only responses. For calculation of KD and other kinetic parameters the Langmuir 1:1 model was used.

Assessment of Ang-2 binding

Binding of indicated antibodies to human Ang-2-RBD-Fc was investigated by surface plasmon resonance using a BIACORE® T200 instrument (GE Healthcare). Around 8000 (RU) of goat anti human F(ab')2 (10 µg/ml anti human F(ab')2; Order Code: 28958325; GE Healthcare Bio-Sciences AB, Sweden) were coupled on a Series S CM5 chip (GE Healthcare BR-1005-30) at pH 5.0 by using an amine coupling kit supplied by the GE Healthcare. HBS-N (10 mM HEPES, 150 mM NaCl pH 7.4, GE Healthcare) was used as running buffer during the immobilization procedure. For the following kinetic characterization, sample and running buffer was PBS-T (10 mM phosphate buffered saline including 0.05% Tween20) at pH 7.4. The flow cell was set to 25°C – and the sample block set to 12°C – and primed with running buffer twice prior to kinetic characterization.

The bispecific antibody was captured by injecting a 5 nM solution for 25 s at a flow of 5 µl/min. The association was measured by injection of human Ang-2-RBD-Fc at various concentrations in solution for 120 s at a flow of 30 µl/min starting with 100 nM in 1:3 serial dilutions. The dissociation phase was monitored for up to 180 s and triggered by switching from the sample solution to running buffer. The surface was regenerated by 60 s washing with a Glycine pH 2.1 solution at a flow rate of 30 µl/min. Bulk refractive index differences were corrected by subtracting the response obtained from a goat anti human F(ab')2 surface. Blank injections are also subtracted (= double referencing). For calculation of apparent KD the Langmuir 1:1 model was used.

Crystallization

Prior to crystallization the Fab protein was concentrated to 20–26 mg/ml in a buffer containing 200 mM CHES pH 9.0, 150 mM NaCl. Initial crystallization trials were performed in sitting drop vapor diffusion setups at 21°C. Crystals appeared within 2 days out of 0.1 M MES, pH 6.5, 20% PEG2000 MME after cross-seeding of droplets. Plate shaped crystals grew within 1 week to a final size of 10 × 200 × 300 µm.

Structure determination and refinement

For data collection crystals were flash cooled at 100 K in precipitant solution containing 10% ethylene glycol. Diffraction data were collected at a wavelength of 1.0000 Å using a PILATUS 6 M detector at the beamline X10SA of the Swiss Light Source (Villigen, Switzerland). Data were processed and scaled with XDS (Kabsch, 2010) and SADABS (Bruker AXS Inc, Madison, 2009). The data+ belong to the space group P1 with cell axes of a = 59.56 Å, b = 59.80 Å, c = 79.09 Å. The resolution limit as obtained was 1.88 Å. The structure was determined by molecular replacement with PHASER (McCoy *et al.*, 2007) using coordinates of an in-house Fab fragment structure as search model. The asymmetric unit contains two Fab molecules. Programs from the CCP4 suite (1994) and Buster (Bricogne *et al.*, 2011) were used to subsequently refine the model. Manual rebuilding of the structure using difference electron density was done with COOT (Emsley *et al.*, 2010). Data collection and refinement statistics for both structures are summarized in Supplemental Table II. Coordinates are deposited in RCSB under the PDB ID 6GHG.

Molecular modeling

Based on the crystal structure of the KK–EE (light chain K123, K124, heavy chain E147, K213; positions given in EU numbering) charge variant non-crossed Fab, the following intermediate charge variants were modeled: KQ–EK, KQ–KE, EK–EK and EK–EK. First, the sidechain types were exchanged where necessary. Afterwards, the sidechain conformers of residues at positions 123, 124 (light chain) and 147, 213 (heavy chain) were optimized simultaneously to attain a maximum number of favorable and a minimal number of unfavorable interactions, the latter including steric clashes. Rotamer optimization was performed using the Dunbrack rotamer library (Shapovalov and Dunbrack, 2011), plus the original rotamers as found in the crystal structure. The rotamer-optimized models were used as starting coordinates for unrestrained energy minimization using the CHARMM36 (Huang and MacKerell, 2013) force field in combination with the GBSW implicit solvent model (Im *et al.*, 2003) and the 'Smart Minimizer' protocol (steepest descent followed by conjugate gradient (Luenberger, 1973) for 500 integration steps. All molecular modeling and simulation was done with BIOVIA Discovery Studio 4.5 (Dassault Systèmes BIOVIA Discovery Studio 4.5, San Diego).

Results

For proof-of-concept, we generated the three possible domain crossover antibodies (as described (Schaefer *et al.*, 2011; Klein *et al.*, 2016) with target specificities directed against Angiopoietin 2 (Ang-2) and Vascular Endothelial Growth Factor (VEGF-A) based on the parental antibodies Ang-2i-LC06 (Thomas *et al.*, 2013; Scheuer *et al.*, 2016) and bevacizumab (Presta *et al.*, 1997; Ferrara *et al.*, 2004) on a human IgG1 framework with knobs-into-holes including an additional stabilizing disulfide bond between the CH3 (constant heavy 3) domains (Merchant *et al.*, 1998; Carter, 2001; Kuglstatter *et al.*, 2017). The domain crossover was introduced into the VEGF binding arm using the described elbow sequence (Klein *et al.*, 2016) together with the knob (T366W) and an additional cysteine (S345C), whereas the hole (T366S, L368A, Y407V) was introduced into the CH3 domain of the Ang-2 binder together with an additional cysteine (Y349C). The antibodies containing the Fab, VH–VL and CH1–CL domain exchange were transiently expressed using four plasmids encoding the respective light chain, the 'crossed light chain', the 'crossed' knob heavy chain and the hole heavy chain as previously described (Schaefer *et al.*, 2011). The different CrossMabs were purified using Protein A chromatography and preparative SEC and analyzed by CE-SDS, SEC and mass spectrometry after each purification step. All three CrossMabs expressed well and represent the main product/peak as demonstrated in this experiment. The analysis of the side products for the Ang-2-VEGF Fab domain crossover antibody revealed a one-armed monovalent non-functional antibody (knob-hole antibody without light chains; Fig. 1A) and a non-functional Fab

(VEGF HC-Fab and Ang-2 LC) which together amounted to 49% (sum). In addition to the correct bispecific antibody, the VH–VL domain crossover antibody expression yielded a side product with twice the non-crossed Ang-2 light chain on both arms of the antibody based on a 'Bence-Jones like' non-cognate pairing of the uncrossed light chain with the crossed VEGF heavy chain (VL–VL interaction). This side product occurred in amounts of up to 20% (Fig. 1B). For the CrossMab$^{CH1–CL}$ no non-cognate light chain pairing was observed (Fig. 1C). An observed side product was an antibody lacking the crossed light chain despite the used equimolar ratios of the plasmids encoding the four different chains.

The existence of side products of the CrossMab^{Fab} and CrossMab$^{VH–VL}$ suggested a need for further improvements to specificity by making the CH1–CL interactions selective for the knob and hole sides of the antibody. One way to achieve correct chain pairing is by the introduction of charged amino acids which make an interaction attractive in case of opposite charges and repulsive in case of identical charges. Previously, this was approached by introducing novel charged residue pairs (Lewis *et al.*, 2014; Liu *et al.*, 2015) in the CH1–CL interface in suitable positions. The approach described herein uses existing charge pairs and selectively is achieved by inverting the existing charge pairs. For this purpose, we searched for existing pairwise electrostatic interactions between residues in the CH1–CL interface and identified the positions E123 and Q124 for Cκ and E123 and E124 for Cλ in the light chain and K147 and K213 in the CH1 (Fig. 2 and Supplemental Fig. 1). An inversion of these charge pairs on the hole side of the antibody by introducing K or R as positively charged amino acids and E or D as negatively charged amino acid or the introduction of a new charge pair in the case of Q124, respectively (on the knob side) should lead to attractive interactions in case of cognate light chain assembly and to repulsive interactions in case of incorrect assembly. Thus, these modifications are intended to enforce correct light chain assembly.

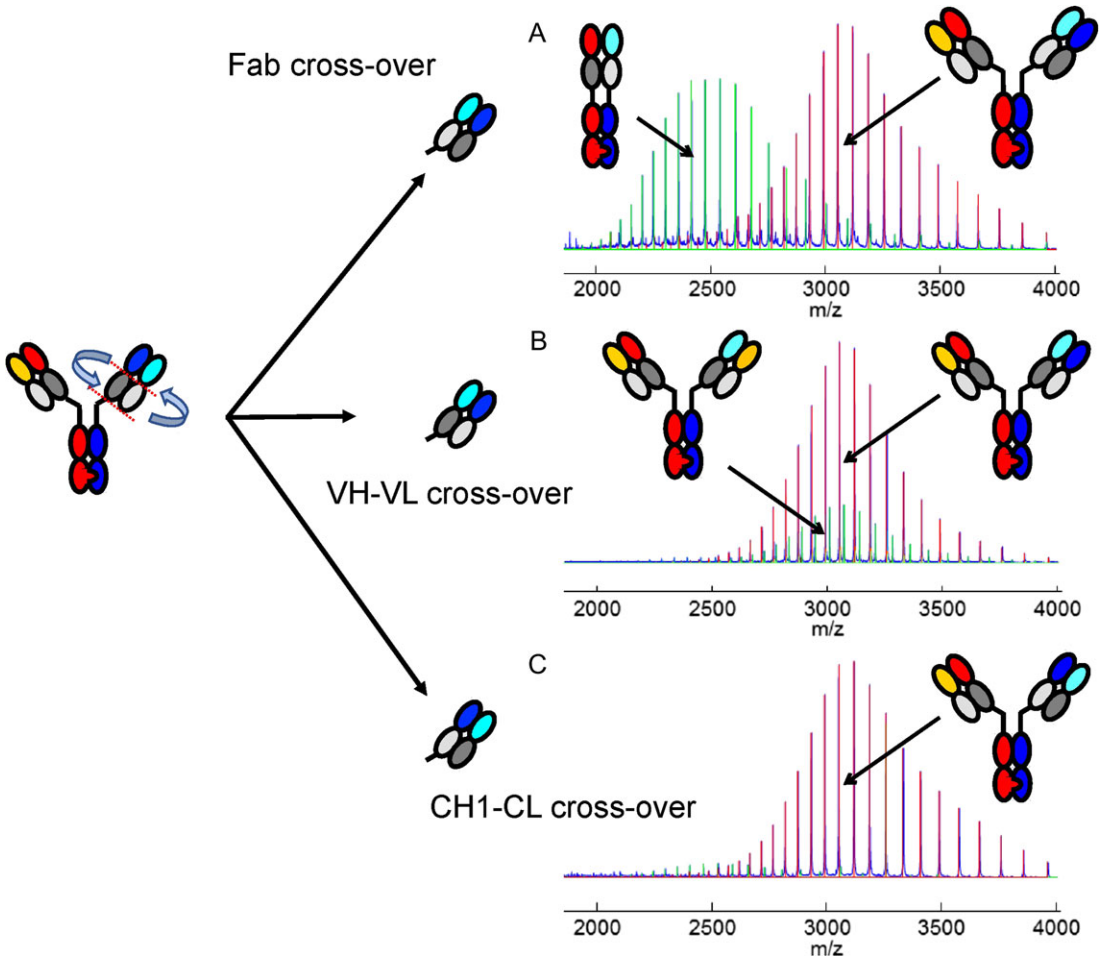

Fig. 1 Possible domain crossovers to generate bispecific antibodies and the observed side products. A bispecific antibody consists of two light and two heavy chains. The knobs-into-holes technology ensures correct heavy chain assembly. The domain crossover ensures correct light chain assembly. The gray colors indicate the similarity of constant domains in both Fab arms. There are three possibilities for this cross-over, as indicated by the red dotted cutting lines. The CrossMab^{Fab} cuts N-terminally of the hinge region and translocates the light blue light chain into the former position of the heavy chain. The CrossMab$^{VH–VL}$ cuts between the constant and variable domains (elbow) and translocates the VH domain into the former position of the VL domain and vice versa. Total mass determination by UHR-ESI-QTOF mass spectrometry of the cross-over bispecific antibody formats (**A**) CrossMab^{Fab}, (**B**) CrossMab$^{VH–VL}$, (**C**) CrossMab$^{CH1–CL}$ with observed major side products. The CrossMab^{Fab} and CrossMab$^{VH–VL}$ formats result in a non-functional monovalent antibody, and an antibody with two identical non-crossed light chains (orange/light gray) formed by a Bence-Jones like interaction, respectively. In many cases no side products are observed using the CrossMab$^{CH1–CL}$ format.

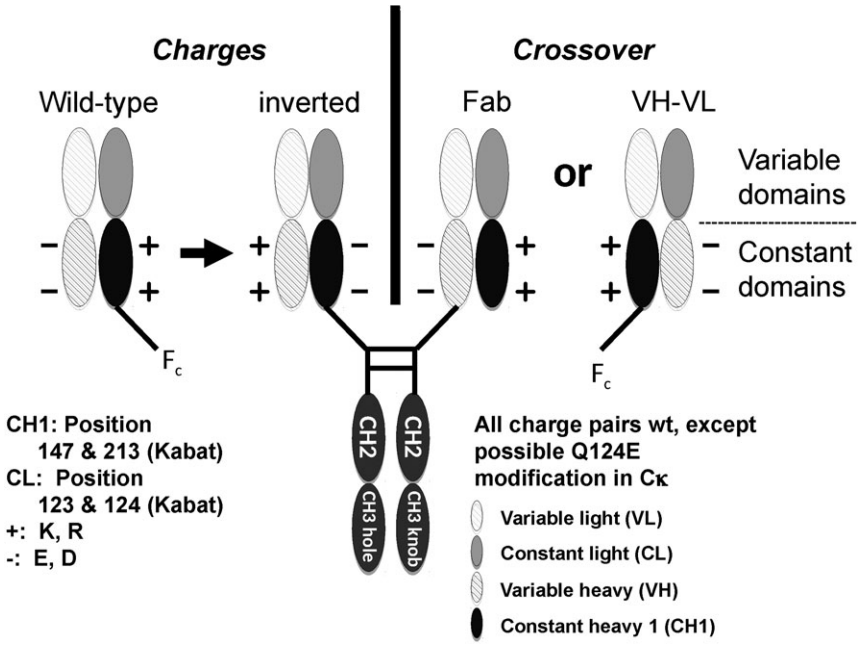

Fig. 2 The approach used herein to make the strong CH1–CL interactions selective for each heavy chain or side of the antibody is the inversion of existing salt bridges or opposite charge pairs (inversion of +(K) to –(E)). The selected charge pairs are depicted on the left. The numbering is according to Kabat. The domain cross-over changes the symmetry of one Fab arm and enables a selective fit (right drawing). Inverted charge-pairs in CH1–CL induce attractive and repulsive forces. Both modifications together enforce correct light chain assembly on each side of the bispecific antibody. Additional exchanges (e.g. D instead of E, R instead of K) are listed in Tables II–IV and VI.

Table II. Overview of Ang-2-VEGF CrossMab$^{VH–VL}$ with 0, 1 and 2 charge pair inversions and their influence on correct light chain assembly

Molecule # (Ang2-VEGF-)	Ang-2-Fab		Crossed VEGF Fab		'Bence Jones like' non-cognate LC pairings by MS [%]
	LC (123/124)	HC (147/213)	LC (123/124)	HC (147/213)	
0273 (wt)	EQ	KK	EQ	KK	20
0394	KQ	EK	EQ	KK	15
0395	KQ	KE	EQ	KK	15
0396	EK	EK	EQ	KK	3
0397	EK	KE	EQ	KK	3
0282	KR	EE	EE	KK	0
0283 (lambda)	KK	EE	EQ	KK	0
0284	KR	ED	EQ	KK	0
0285 (Q124E in crossed VEGF Fab)	KR	ED	EE	KK	0
0286	KK	EE	EE	KK	0

Charge exchanged CrossMab$^{VH–VL}$

To test this hypothesis, the respective Ang-2-VEGF CrossMab$^{VH–VL}$ was generated with the inverted charged pairs on the Ang-2 side (knob): E123→K, Q124→K in the CL domain and K147→E and K213→E in the CH1 domain, whereas the crossed VEGF Fab arm (hole) remained unchanged. Expression yields and the side products were compared with a parallel expression of the Ang-2-VEGF CrossMab$^{CH1–CL}$ without charge exchanges. The yield increased twofold and no side products or missing light chains could be detected (data not shown).

Based on this promising initial result, the next logical step was to assess the influence of each individual charge (Table II). The basis for the evaluation was the CrossMab$^{VH–VL}$ without any charged residue exchanges which shows a 'Bence-Jones-like' non-cognate light chain pairing with about 20% (wt Ang-2 light chain in two copies, described above) (Fig. 3, Table II).

Data from constructed homology models or available X-ray structures at that time did not provide clear hints to which of the selected positions in the light chain interacts with the corresponding charged residue in the heavy chain (Supplemental Fig. 1). Probing each combination individually and assessing its influence on the side product profile aimed to identify the key interactions and their contributions. The first charge pair to be inverted was the position E123→K in the CL which could potentially form a salt bridge with K147→E or K213→E in the CH1. These modifications reduced the amount of the CrossMab with two Ang-2 light chains from 20% to about 15% as quantified by mass spectrometry (0394 & 0395 in Fig. 3). Modifying position Q124→K in the light chain and probing it with the K147→E and or K213→E mutations reduced the side product amount down to 3% (0396 & 0397 in Fig. 3). The combination of E123→K and Q124→R in the light chain and K147→E and K213→D in the heavy chain reduced the amount of side products below the detection limit

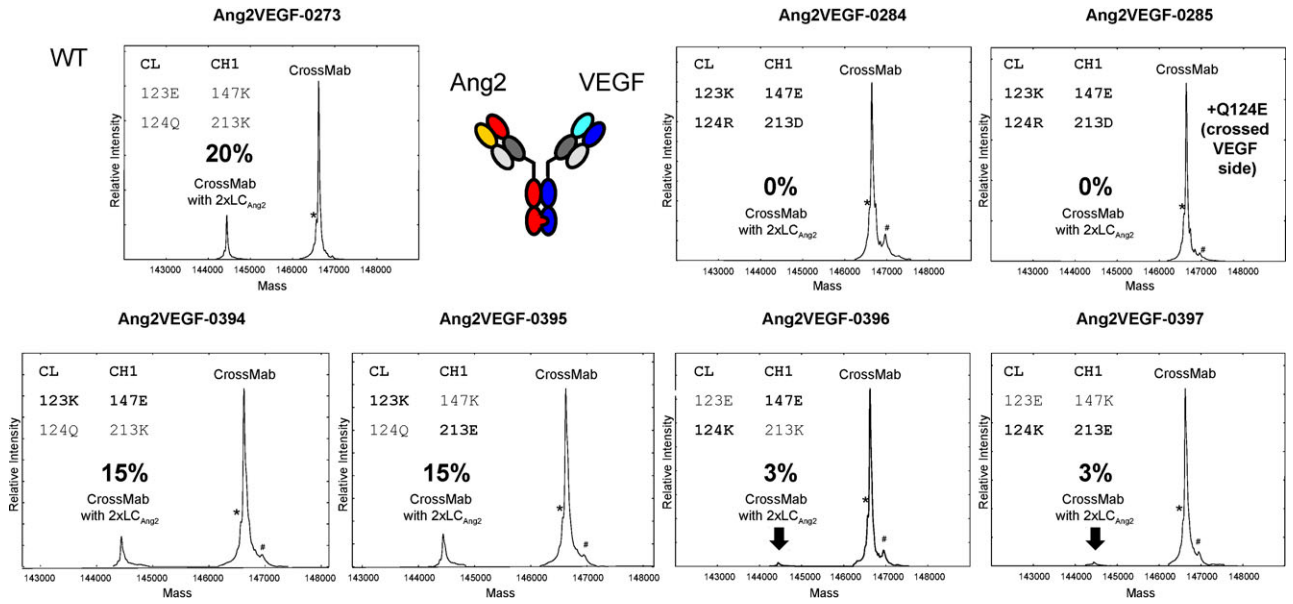

Fig. 3 Side product quantification for the CrossMab$^{VH–VL}$ (Bence-Jones like side product) in dependency of individual charge pair exchanges. The influence of each individual charge exchange, its position and pairing preference can be visualized by comparing and quantifying the MS signals for the cognate light chain assembly and the Bence-Jones like assembly, i.e. two Ang2 light chains (% in bold). The charge pair inversion is always on the wt Fab arm. For Ang2VEGF-0285 two charge pairs were exchanged on the Ang2 arm and one additional charge (Q124E) is added on the crossed VEGF arm. *HC wo C-term. glycine; #phosphate adduct.

Table III. Overview on Tweak-IL17 CrossMab$^{VH–VL}$ with 0 and 2 charge pair inversions and its influence on correct light chain assembly

Molecule # (TweakIL17-)	IL17 Fab		Crossed Tweak Fab		'Bence Jones like' non-cognate LC pairings by MS [%]
	LC (123/124)	HC (147/213)	LC (123/124)	HC (147/213)	
0096 (wt)	ED	KK	EQ	KK	~20
0097 (Q124E in crossed Tweak Fab)	RK	EE	EE	KK	0
0098	RK	ED	EQ	KK	0
0099 (Q124E in crossed Tweak Fab)	RK	ED	EE	KK	0
0100 (Q124E in crossed Tweak Fab)	KK	EE	EE	KK	0

by mass spectrometry (0284 & 0285 in Fig. 3). Also, combinations of E123→K and Q/E124→K or R (including lambda), and K147→E and K213→E did not show any side products (Table II). The beneficial impact of the position Q124 in kappa light chains and E124 in lambda light chains suggests modifying position 124 in the crossed VEGF CL domain for kappa light chains with a Q→E exchange. An additional benefit for the Ang-2-VEGF CrossMab$^{VH–VL}$ could not be shown as already no side products occurred in the case of two inverted charge pairs in the wt Ang-2 chain (0285 in Fig. 3; Table II). Nevertheless, there was no loss of selectivity or stability observed with it. Finally, no impact on target binding was observed in the correctly assembled CrossMab as determined by SPR-based binding assays. The affinity towards both targets was not altered within the precision of these measurements. Likewise, there was no significant impact on the thermal stability as measured as T_{agg} (°C) or T_m (°C) for all generated variants. All CrossMab$^{VH–VL}$ with one or two charge pair inversions and the optional Q124E modification in CL of the crossed Fab arm showed T_{agg} in a range between 56°C and 57°C and T_m in a range between 61°C and 62°C. The data of the charge pair exchanges and their impact on non-cognate light chain pairing are summarized in Table II and Supplemental Table I.

To demonstrate the general suitability of the newly identified charged residue bispecific CrossMab$^{VH–VL}$ antibodies with different target specificities were evaluated. As a first example, a bispecific antibody targeting the two soluble ligands Tweak (Lammens *et al.*, 2013) and IL-17 (Fischer *et al.*, 2015) for use in inflammatory indications was generated. The initial CrossMab$^{VH–VL}$ showed ~20% 'Bence Jones like' non-cognate light chain as quantified by mass spectrometry (Table III). The introduction of two inverted charged residue pairs in position CL E123→R or K and D124→ K and CH1 K147→E and K213→E or D resulted in a correctly assembled bispecific antibody without formation of detectable side products. An additional charge correction in the crossed light chain (Q124E) did not show additional benefits (Table III).

As a second example, a trispecific c-Met/HER1/3 Cross-DAF (DAF = dual action Fab) for potential use in oncology was tested. In this trispecific antibody (Klein *et al.*, 2016) one target binding Fab is directed against c-Met (Merchant *et al.*, 2013) whereas the other is a dual acting Fab capable of binding either HER1 or HER3 (Eigenbrot and Fuh, 2013). The corresponding CrossMab$^{VH–VL}$ showed only trace impurities of a non-cognate light chain, nevertheless, the introduction of the charged residues in one or both Fab arms removed any incorrect light chain assembly (Table IV).

Table IV. Overview on c-Met-Her1/3 CrossDAF$^{VH–VL}$ with 0, and 2 charge pair inversions and their influence on correct light chain assembly

Molecule # (MetHER1(3)DAF-)	Her DAF		Crossed cMet Fab		'Bence Jones like' non-cognate LC pairings by MS [%]
	LC (123/124)	HC (147/213)	LC (123/124)	HC (147/213)	
0004 (wt)	ED	KK	ED	KK	Trace amounts
0005	RK	ED	ED	KK	0
0006 (Q124E in crossed cMet Fab)	RK	ED	EE	KK	0

Table V. Overview of Ang-2-VEGF CrossMab^{Fab} with 0 and 2 charge pair inversions and their influence on correct light chain assembly

Molecule # (Ang2VEGF-)	Ang-2-Fab		Crossed VEGF Fab		'HC-dimer' formation by CE-SDS [%]
	LC (123/124)	HC (147/213)	LC (123/124)	HC (147/213)	
289 (wt)	EQ	KK	EQ	KK	40
280	KK	EE	EQ	KK	27
111 (Q124E in crossed VEGF Fab)	KK	EE	EE	KK	19
290 (lambda, wt)	EE	KK	EE	KK	30
279 (lambda)	KK	EE	EE	KK	14

Table VI. Non-covalent canonical state of the pairwise interactions between E123 of the light chain and K213 heavy chain and E/Q214 of the light chain and K147 of the heavy chain based on publicly available high-resolution X-ray structures of CH1–Cκ ($n = 50$, resolution ≤1.8 Å) and CH1–Cλ ($n = 26$, resolution ≤2.0 Å) from the Protein Data Bank

	Residue pair (light chain-heavy chain)	Interaction found (Discovery Studio)	Salt bridge	Attractive charge
CH1–Cκ	E123–K213	46/50	29/46	17/46
$n = 50$	Q124–K147	0/50	–	–
CH1–Cλ	E123–K213	19/26	11/26	8/26
$n = 26$	E124–K147	24/26	7/24	17/24

All deglycosylated CrossMabs were analyzed in their intact state by mass spectrometry and were also evaluated following an additional limited digestion with endoprotease LysC to generate Fab fragments. The purpose of this additional evaluation was to exclude the presence of any non-cognate side products with both the crossed and uncrossed LCs misassembled with the HCs within one CrossMab molecule. In that case, the correctly and incorrectly assembled intact CrossMabs would be isobaric. The analysis of all LysC generated Fabs excluded the presence of this kind of side product (data not shown).

Charge exchanged CrossMab^{Fab}

The use of the CrossMab^{Fab} is impeded by the formation of a heavy chain dimer containing a non-functional binding domain comprised of two variable domains with different target specificity. Reversing the charge interaction of existing charge pairs in the CH1–CL domains as described for the CrossMab$^{VH–VL}$ could improve this design by reducing the amount of HC-dimer. Therefore, we evaluated the influence of two charge-pairs in a kappa–kappa and a lambda–kappa CrossMab^{Fab}. While the results of this approach evidently showed a beneficial influence, the overall effect was not big enough to completely eliminate the HC-dimer formation (Table V). The HC-dimer occurred in amounts of 40% in the wt kappa–kappa CrossMab^{Fab} and could be reduced to about 20% as measured by CE-SDS under non-reducing conditions. By introduction of two inverted charge pairs in the non-crossed CH1–CL interface, the amount of this side product could be reduced to 14% (Table V). Taken together, the overall effect on the formation of the correct CrossMab^{Fab} products was not big enough to eliminate the undesired heavy chain dimer side product.

X-ray structure of the KK–EE charge variant non-crossed Fab and modeling of intermediate charge variants

To establish a structure function relationship further and to correlate the experimental results to structural information, the Fab fragment of a non-binding germline antibody with GS motif containing CDR residues in the heavy chain CDR3 termed DP47 with the charged residue inversion KK–EE described above was crystallized and the X-ray structure solved. Fig. 4 shows the respective crystal structure with the mutated charge interactions (Fig. 4A, PDB code 6GHG) in context with two high-resolution CH1–Cκ and CH1–Cλ X-ray structures representing the respective wildtypes (Fig. 4B, left: PDB code 4XAW at 1.47 Å resolution (Irimia *et al.*, 2016); Fig. 4B right: PDB code 4LLD at 1.19 Å resolution (Lewis *et al.*, 2014)).

To investigate the canonical state of the pairwise interactions between E123 of the light chain and K213 heavy chain and E/Q214 of the light chain and K147 of the heavy chain, we collected a number of publicly available high-resolution X-ray structures of CH1–Cκ ($n = 50$, resolution ≤1.8 Å) and CH1–Cλ ($n = 26$, resolution ≤2.0 Å) from the Protein Data Bank and monitored the non-covalent interactions using BIOVIA Discovery Studio. The results are shown in Table VI.

In the case of CH1–Cκ, the interaction E123–K213 is a highly conserved salt bridge or (in case of longer distances) attractive charge pair interaction. By contrast, there seems to be no conserved

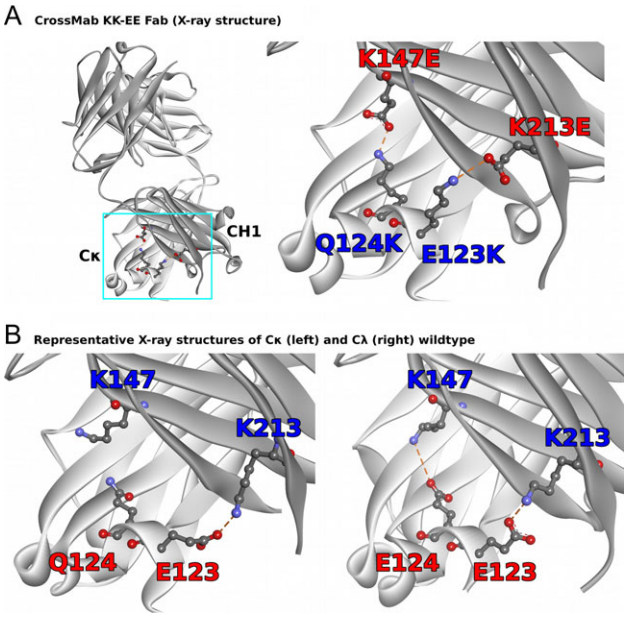

Fig. 4 (**A**) X-ray structure of the DP47 Fab with the inverted charge pairs E123K, Q124K, K147E and K213E (left) and close-up on the mutated residues in the CH1 and Cκ domains (right). (**B**) Cross-chain interactions involving residues at the same positions in two representative high-resolution X-ray structures of CH1–Cκ wildtype (PDB code 4XAW, left) (Irimia *et al.*, 2016) and CH1–Cλ wildtype (PDB code 4LLD) (Lewis *et al.*, 2014).

interaction between residues Q124 and K147. In the case of CH1–Cλ, the number of high-resolution X-ray structures is limited, but the available structural data suggests that there are conserved interactions between the pairs E123–K213 and E124–K147, either in the form of salt bridges or longer distance attractive charge pairs.

In the X-ray structure of the CrossMab KK–EE charge variant of the DP47 Fab (PDB ID 6GHG, Fig. 5B) the two pairs 123–213 and 124–147 form salt bridges. This holds for both copies of the Fab that can be found in the asymmetric unit of the crystal structure. The configuration is thus more similar to the two interacting glutamic acid-lysine pairs in the CH1–Cλ wildtype Fab (Fig. 4B right) than to the CH1–Cκ wildtype Fab, where only the E123–K213 salt bridge seems to be conserved (Fig. 5A).

In comparison to the wildtype, the polarity is reversed and accentuated: The positively charged residues are moved from the heavy chain to the light chain side, while the negatively charged residues are moved from the light chain to the heavy chain side, and in this process are made more negative by replacing the glutamine with glutamic acid (in Cκ). Cκ–CH1 pairing with chains that carry the canonical charge configuration is thus rendered energetically unfavorable. This could apply not only with regard to putative direct interactions between the two residue pairs, but also affect general electrostatic steering during the assembly of the encounter complex.

To evaluate the structural implications of partial charge exchange (only one residue per chain), we modeled the intermediate variants KQ–EK, KQ–KE, EK–KE, and EK–EK (always residue 123, 124–147, 213) as assessed experimentally and studied the potential pairing interactions. These variants are shown in Fig. 5C–F). For the variants KQ–KE and EK–EK, we found favorable pairwise interactions between both 123–213 and 124–147. By contrast, for the variants KQ–EK and EK–KE, our modeling predicts no inter-chain interactions involving the four residues. In the case of EK–KE (Fig. 5E), the obvious reason is that the pairs 123–213 and 124–147 possesses the same charge and hence lead to mutual repulsion. In the case of KQ–EK (Fig. 5C), hydrogen bonding between Q124 and E147 is conceivable; however, the model suggests that the opposing glutamine and glutamic acid side chains are not long enough to form the inter-chain hydrogen bond. Instead, the side chain amine of Q124 prefers to interact with its own backbone carbonyl group. The remaining K123 and K213 pair is repulsive. In all of the cases, we only observed interactions between the residues at positions 123 and 213 and between the residues at positions 124 and 147, and not the hypothetical crosswise interactions 123–147 or 124–213.

Discussion

Human bispecific heterodimeric IgG-format antibodies have paved their way from early research to clinical development and recently with the approval of emicizumab (Kitazawa *et al.*, 2017; Oldenburg *et al.*, 2017). One of the key challenges for large scale pharmaceutical production of similar bispecific antibodies is the correct assembly of all chains. Currently, there are very few technologies available which ensure this prerequisite. The common light chain approach as applied for emicizumab utilizes two heavy and one common light chain to generate the bispecific molecule. This approach is straightforward and works well. Nevertheless, it does not allow the use of existing antibodies pairs, and the identification of a suitable common light chain can be challenging (Sampei *et al.*, 2013). For antibodies consisting of four individual chains the challenge remains to enable correct light chain assembly. Recently, novel orthogonal Fab interfaces were generated by a combined *in silico* and screening approach (Lewis *et al.*, 2014; Liu *et al.*, 2015; Bonisch *et al.*, 2017). Challenges in case of non-cognate light chain pairings during cell-line and process development may occur as the similarity with regards to the biophysical properties of the two different Fab arms can be very high. Nevertheless, this approach is predicted to work well and the potential challenges maybe circumvented by novel approaches in cell-line development like targeted integration. A common and well-established work around is a sophisticated and tailored purification strategy to enable pharmaceutical grade quality even for non-completely self-assembling bispecific antibodies (Smith *et al.*, 2015).

We chose a novel strategy combining the CrossMab technology with selected charge pairs in order to disable the formation of undesired side products for the VH–VL and the Fab arm crossover (Schaefer *et al.*, 2015; Imhof-Jung *et al.*, 2016). For the CrossMab$^{CH1–CL}$ non-cognate light chain pairing does not occur. The challenge can be the weaker expression of the crossed light chain, leading to an antibody lacking the crossed light chain. This might be explained by the missing BiP chaperone interaction during the secretion of the antibody out of the cell (Feige *et al.*, 2009). The correct domain order for interaction with BiP is given for the remaining two CrossMab designs as the CH1 domain is part of the heavy chain. For the CrossMab$^{VH–VL}$, the main side product is a 'Bence-Jones like' VL–VL interaction, which is hard to separate from the bispecific antibody with chromatographic methods. In theory, the CrossMab^{Fab} is the most preferred CrossMab design, as it utilizes only one non-natural domain exchange/transition, which does not impact stability and assembly and no modified elbow linker regions. Even though we did not manage to find a way to completely prevent the non-cognate VH–VL interaction in the CrossMab^{Fab}, this side product of a monovalent non-functional antibody can be easily removed by chromatographic methods due to the difference in molecular weight.

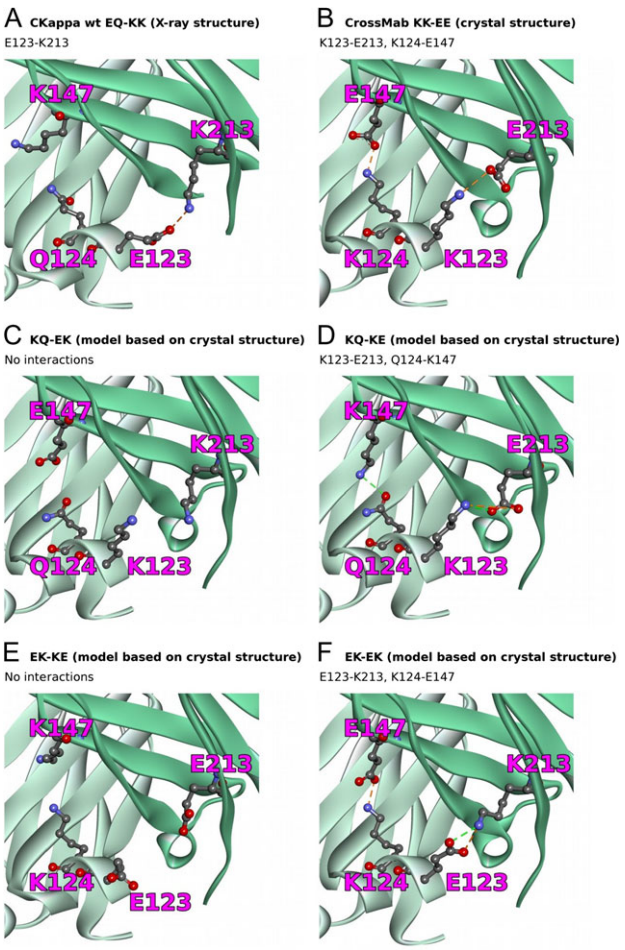

Fig. 5 Electrostatic interactions between the residues at light chain positions 123 and 124 and heavy chain positions 147 and 213 in the X-ray structure of the canonically paired CH1–Cκ wildtype Fab (**A**, PDB code 4XAW) (Irimia *et al.*, 2016) and in the crystal structure of the KK–EE charge variant Fab (**B**, PDB code 6GHG). The results of the modeling of individual charge-pair interactions (using structure 6GHG as starting configuration) are depicted in panels **C**–**F**. The light chain is shown in light green, the heavy chain in dark green. Residue numbers are given in EU numbering.

Notably, all side products possess the wildtype CH1–CL interaction, whereas a Bence-Jones like VL–VL interaction is observed for the VH–VL crossover and a non-cognate VH–VL is observed for the CrossMab^{Fab}. Based on this experimental result, it can be concluded that the driving force for correct light chain localization is the strong CH1–CL interaction (at least for antibodies without stability engineered VH–VL domains).

Some additional conclusions can be drawn from the results of the described experiment. First, the interaction between VL–VL is not repulsive enough to enforce correct light chain assembly in the CrossMab$^{VH–VL}$. Second, the interaction between VH–VL of non-cognate domains originating from different target binders/germlines is not repulsive enough to enforce cognate light chain assembly or to overcome the CH1–CL pairing preference in the CrossMab^{Fab}. Third, the driving force for correct light chain assembly is in all three CrossMabs the strong CH1–CL interaction.

The focus of the work described here was the optimization and development of a completely self-assembling bivalent bispecific antibody expressed by four individual chains, two light and two heavy chains. The CrossMab$^{VH–VL}$ design including inverted charge pairs in CH1–CL of the non-crossed chain represents such a system ensuring error-free self-assembly in a modular system based on available antibody pairs, allowing the use of notably, any preexisting antibody. The solved X-ray structure illustrates the effect of the two charge pair exchanges/inversions and shows the corresponding electrostatic interactions, namely 123–213 and 124–147 independent of the applied charges. The effect of each individual charge pair exchange is difficult to interpret, as the effects on the complete self-assembly are manifold. In our experiments we observed a higher expression level of the non-crossed light chain, resulting only in non-cognate light chain assembly on the crossed Fab arm. The amount and impact of these kinetic effects is not understood. The influence of attractive interactions like salt bridges and hydrogen-bond interactions on the stabilization of a cognate Fab arm as well as repulsive effects originating from similar charges need to be considered on both Fab arms including cognate and non-cognate pairing of each possible Fab arm combination. Importantly, the optimal effect can be achieved by introduction of only two charge pair inversions. This may be caused by a beneficial impact due to similar charges on neighboring residues, resulting in a larger charged surface area, strengthening attractive and repulsive forces. In addition, the two charge pair exchanges result in only attractive interactions for cognate pairing and always repulsive interactions for non-cognate pairing in the CrossMab$^{VH–VL}$. This observation is the main difference to the CrossMab$^{VH–VL}$ without charge pair exchanges, where all wild-type charge pair interactions (123–213, 124–147, cognate and non-cognate) are attractive.

According to the structural model and the experimental results we can provide the following recommendations for preferred CrossMab$^{VH–VL}$ design: First, include the domain crossover on the side of the more stable Fab arm. Second, the inverted charge pairs are preferred to be put on the non-crossed Fab arm. Third, it is favored to apply the knobs-into-holes approach in combination with an additional disulfide bridge, while the knob-side is located on the crossed half of the antibody. It is recommended to correct the position Q124 in Cκ to E in addition.

In summary, the CrossMab$^{VH–VL}$ with inverted charge pairs is a mature bispecific design, allowing the combination of individual target binding domains in an IgG-like molecule utilizing 1 + 1, 1 + 2 or 2 + 2 target binding sites as required from the biological point of view. The potential of the CrossMab technology is reflected by the number of bispecific molecules in preclinical and clinical development (Klein *et al.*, 2016; Brinkmann and Kontermann, 2017; Verdino *et al.*, 2018). Currently there are already two trivalent heterodimeric 2 + 1 T-cell bispecific antibodies utilizing the CrossMab$^{VH–VL}$ design with charge pair inversions targeting CD20 (Bacac *et al.*, 2018) and BCMA (Seckinger *et al.*, 2017) in Phase 1 early clinical development. This demonstrates the maturity of the CrossMab$^{VH–VL}$ design with inverted charge pairs and CrossMab technology. The ability to combine 1 + 1, 1 + 2 and 2 + 2 target binding sites in one molecule enables to make use of affinity or avidity driven target binding to enable control over (cell-) selectivity and biodistribution.

Supplementary data

Supplementary data are available at *Protein Engineering, Design and Selection* online.

Acknowledgements

The authors thank their management for continuous support and sponsorship. We thank Anton Jochner, Xaver Reiser, Manuel Endesfelder, Achim Gärtner and Alexandra Kaczmarek for material supply and experimental support.

References

Bacac,M., Colombetti,S., Herter,S. *et al.* (2018) *Clin. Cancer Res.* doi: 10.1158/1078-0432.CCR-18-0455

Bacac,M., Fauti,T., Sam,J. *et al.* (2016a) *Clin. Cancer Res.*, **22**, 3286–3297.

Bacac,M., Klein,C. and Umana,P. (2016b) *Oncoimmunology*, **5**, e1203498.

Bonisch,M., Sellmann,C., Maresch,D., Halbig,C., Becker,S., Toleikis,L., Hock,B. and Ruker,F. (2017) *Protein Eng. Des. Sel.*, **30**, 685–696.

Bricogne,G., Blanc,E., Brandl,M. *et al.* (2011) *Buster version 295*. Global Phasing Ltd, Cambridge, United Kingdom.

Brinkmann,U. and Kontermann,R.E. (2017) *MAbs*, **9**, 182–212.

Brunker,P., Wartha,K., Friess,T. *et al.* (2016) *Mol. Cancer Ther.*, **15**, 946–957.

Carter,P. (2001) *J. Immunol. Methods*, **248**, 7–15.

Chelius,D., Ruf,P., Gruber,P., Ploscher,M., Liedtke,R., Gansberger,E., Hess, J., Wasiliu,M. and Lindhofer,H. (2010) *MAbs*, **2**, 309–319.

Eigenbrot,C. and Fuh,G. (2013) *Curr. Opin. Chem. Biol.*, **17**, 400–405.

Emsley,P., Lohkamp,B., Scott,W.G. and Cowtan,K. (2010) *Acta Crystallogr. D Biol. Crystallogr.*, **66**, 486–501.

Feige,M.J., Groscurth,S., Marcinowski,M., Shimizu,Y., Kessler,H., Hendershot,L.M. and Buchner,J. (2009) *Mol. Cell*, **34**, 569–579.

Fenn,S., Schiller,C.B., Griese,J.J. *et al.* (2013) *PLoS One*, **8**, e61953.

Ferrara,N., Hillan,K.J., Gerber,H.P. and Novotny,W. (2004) *Nat. Rev. Drug Discov.*, **3**, 391–400.

Fischer,J.A., Hueber,A.J., Wilson,S. *et al.* (2015) *Arthritis Rheumatol.*, **67**, 51–62.

Huang,J. and MacKerell, A.D., Jr. (2013) *J. Comput. Chem.*, **34**, 2135–2145.

Igawa,T., Tsunoda,H., Kikuchi,Y. *et al.* (2010) *Protein Eng. Des. Sel.*, **23**, 667–677.

Im,W., Lee,M.S. and Brooks, C.L., 3rd (2003) *J. Comput. Chem.*, **24**, 1691–1702.

Imhof-Jung,S., Klein,C., Klostermann,S., Regula,J.T. and Schaefer,W. (2016) WO2016016299A1: Multispecific antibodies. Patent application.

Irimia,A., Sarkar,A., Stanfield,R.L. and Wilson,I.A. (2016) *Immunity*, **44**, 21–31.

Kabsch,W. (2010) *Acta Crystallogr. D Biol. Crystallogr.*, **66**, 133–144.

Kienast,Y., Klein,C., Scheuer,W. *et al.* (2013) *Clin. Cancer Res.*, **19**, 6730–6740.

Kitazawa,T., Esaki,K., Tachibana,T. *et al.* (2017) *Thromb. Haemost.*, **117**, 1348–1357.

Klein,C., Schaefer,W. and Regula,J.T. (2016) *MAbs*, **8**, 1010–1020.

Klein,C., Sustmann,C., Thomas,M. *et al.* (2012) *MAbs*, **4**, 653–663.

Krah,S., Sellmann,C., Rhiel,L. *et al.* (2017) *N. Biotechnol.*, **39**, 167–173.

Kuglstatter,A., Stihle,M., Neumann,C., Muller,C., Schaefer,W., Klein,C. and Benz,J. (2017) *Protein Eng. Des. Sel.*, **30**, 649–656.

Lammens,A., Baehner,M., Kohnert,U., Niewoehner,J., von Proff,L., Schraeml,M., Lammens,K. and Hopfner,K.P. (2013) *PLoS One*, **8**, e62697.

Lehmann,S., Perera,R., Grimm,H.P. *et al.* (2016) *Clin. Cancer Res.*, **22**, 4417–4427.

Lewis,S.M., Wu,X., Pustilnik,A. *et al.* (2014) *Nat. Biotechnol.*, **32**, 191–198.

Liu,Z., Leng,E.C., Gunasekaran,K. *et al.* (2015) *J. Biol. Chem.*, **290**, 7535–7562.

Luenberger,D.G. (1973) *Introduction to Linear and Nonlinear Programming*. Addison-Wesley Reading, Reading, MA.

McCoy,A.J., Grosse-Kunstleve,R.W., Adams,P.D., Winn,M.D., Storoni,L.C. and Read,R.J. (2007) *J. Appl. Crystallogr.*, **40**, 658–674.

Merchant,M., Ma,X., Maun,H.R. *et al.* (2013) *Proc. Natl Acad. Sci. U S A*, **110**, E2987–E2996.

Merchant,A.M., Zhu,Z., Yuan,J.Q., Goddard,A., Adams,C.W., Presta,L.G. and Carter,P. (1998) *Nat. Biotechnol.*, **16**, 677–681.

Mullard,A. (2017) *Nat. Rev. Drug Discov.*, **16**, 810.

Nagorsen,D., Kufer,P., Baeuerle,P.A. and Bargou,R. (2012) *Pharmacol. Ther.*, **136**, 334–342.

Oldenburg,J., Mahlangu,J.N., Kim,B. *et al.* (2017) *N. Engl. J. Med.*, **377**, 809–818.

Presta,L.G., Chen,H., O'Connor,S.J., Chisholm,V., Meng,Y.G., Krummen,L., Winkler,M. and Ferrara,N. (1997) *Cancer Res.*, **57**, 4593–4599.

Regula,J.T., Lundh von Leithner,P., Foxton,R. *et al.* (2016) *EMBO Mol. Med.*, **8**, 1265–1288.

Regula,J.T., Lundh von Leithner,P., Foxton,R. *et al.* (2017) *EMBO Mol. Med.*, **9**, 985.

Sampei,Z., Igawa,T., Soeda,T. *et al.* (2013) *PLoS One*, **8**, e57479.

Schaefer,W., Klein,C., Imhof-Jung,S., Klostermann,S., Molhoj,M. and Regula,J.T. (2015) WO2015150447A1: Multispecific antibodies. Patent application

Schaefer,W., Regula,J.T., Bahner,M. *et al.* (2011) *Proc. Natl Acad. Sci. U S A*, **108**, 11187–11192.

Schaefer,W., Volger,H.R., Lorenz,S., Imhof-Jung,S., Regula,J.T., Klein,C. and Molhoj,M. (2016) *MAbs*, **8**, 49–55.

Scheuer,W., Thomas,M., Hanke,P. *et al.* (2016) *MAbs*, **8**, 562–573.

Seckinger,A., Delgado,J.A., Moser,S. *et al.* (2017) *Cancer Cell*, **31**, 396–410.

Shapovalov,M.V. and Dunbrack, R.L., Jr. (2011) *Structure*, **19**, 844–858.

Smith,E.J., Olson,K., Haber,L.J. *et al.* (2015) *Sci. Rep.*, **5**, 17943.

Spiess,C., Zhai,Q. and Carter,P.J. (2015) *Mol. Immunol.*, **67**, 95–106.

Thomas,M., Kienast,Y., Scheuer,W. *et al.* (2013) *PLoS One*, **8**, e54923.

Verdino,P., Atwell,S. and Demarest,S.J. (2018) *Curr. Opin. Chem. Eng.*, **19**, 107–123.